S1 Morphological Indices:

As depicted in Fig. S1, the calculation of morphological indices for intracranial aneurysms (IA) entails the precise isolation of each IA sac from its corresponding parent vessel structure[1]. Various geometrical parameters are computed for the isolated aneurysm region after the above-said IA isolation. The following IA geometric characteristics were quantified: volume, height, maximum sac width, vessel diameter, minimum ostium diameter, maximum ostium diameter, aneurysm surface area, and ostium surface area. These variables are summarized in Table S1.

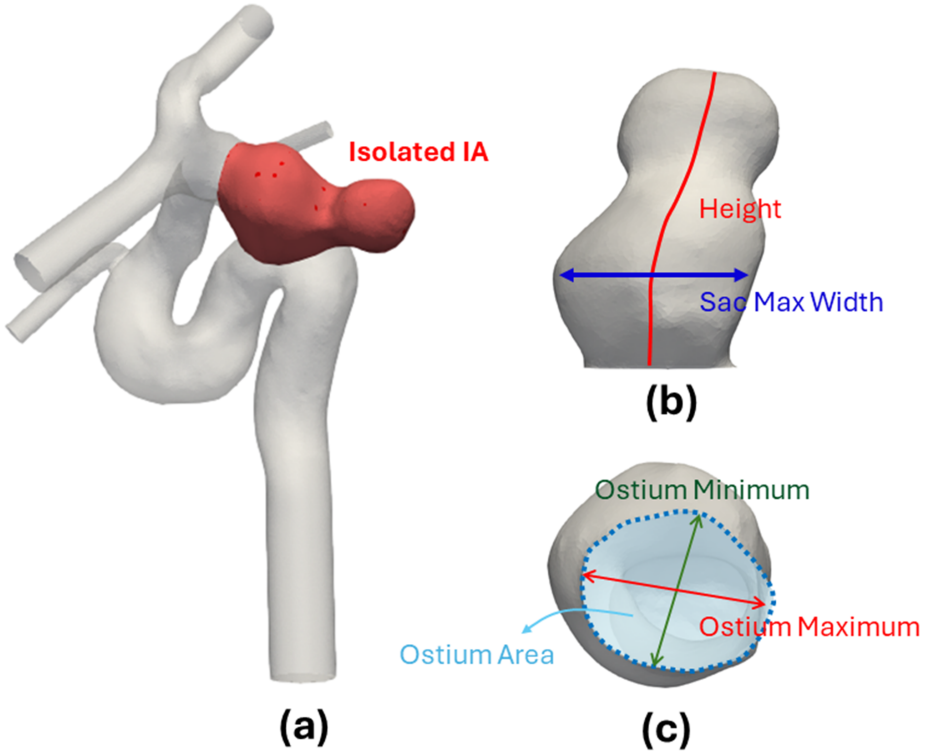

Figure S1. An illustration of the geometric characteristics of typical IAs is provided. (a) shows an isolated IA sac from the parent vessel (highlighted in red). In (b), the solid red lines represent the centerlines generated using the Voronoi diagram[2], where the height of the IA is determined by the length of the centerline within the aneurysm region. The blue line indicates the maximum width of the IA. In (c), the blue circle represents a 2D cutting plane used to measure the minimum and maximum ostium diameters, and the blue surface area on the cutting plane indicates the ostium area.

Table S1. A summary of morphological variable

Parameter	Descriptions
Aneurysm volume	Volume of the aneurysm aneurysm
height	Height of the aneurysm
Sac max width	Maximum width of the aneurysm sac
Size ratio width	The size ratio between aneurysm width and parental artery diameter
Ostium minimum	The maximal ostium diameter
Ostium maximum	The minimal ostium diameter
Aneurysm area	Area of the aneurysm
Ostium area	Area of the ostium

S2 Hemodynamic Indices: wall shear stress

Wall shear stress (WSS) arises from the frictional and tangential forces exerted on the vessel wall by the blood flow. It is quantified as follows[3]:

$$WSS = \mu\dot{\gamma} \tag{1}$$

Where μ is the dynamics viscosity and $\dot{\gamma}$is the share rate.

This study automatically computed WSS utilizing a commercial CFD solver (Fluent, ANSYS Inc., USA). Following the estimation of WSS at each timestep, the extrema (minimum and maximum values) and the spatially averaged WSS were determined. Subsequently, the temporally averaged WSS minimum (TA-WSS-Min), maximum (TA-WSS-Max), spatial average (STA-WSS) and temporally averaged low wall shear ($\leq$ 2 Pa) area (TA-LSA)[4] were calculated.

Additionally, the Oscillatory Shear Index (OSI), a nondimensional parameter indicating the change in direction of WSS, was calculated at each point on the vessel wall. The OSI provides insight into the oscillatory nature of the shear stress experienced by the vessel wall over the cardiac cycle[5], as follows:

$$\mathrm{OSI} = 0.5\left(1 - \frac{\left|\int_0^T \tau_i dt\right|}{\int_0^T |\tau_i| dt}\right) \tag{2}$$

The calculated OSI value ranges from 0 to 0.5, with 0 indicating no directional change in the WSS vector, whereas an OSI value of 0.5 corresponds to a 180° angular change in directionality during a cardiac cycle.

S3 Velocity-Informatiss Indices:

In this study, `velocity-informatics` technique is employed to quantify blood flow characteristics using spatial pattern analysis, as documented in our recent studies[6,7].

This method involves a systematic process comprising four key steps. **First**, an algorithm adapted from previous literature[1], is employed to isolate the velocity field within the aneurysm dome. **Second**, The isolated velocity fields are resampled onto a uniform grid using interpolation techniques, achieving a voxel resolution of $0.2 \times 0.2 \times 0.2$ mm³. **In the third step**, as illustrated in Fig. S2, Utilizing Leopardi's method for equal partitioning of a unit sphere, the sphere's surface is divided into 360 equal segments, each representing a unique partition direction[8]. A partition direction is characterized by a vector originating from the center of the unit sphere and terminating at the centroid of the segment. Each velocity vector within an IA is subsequently assigned to the partition vector that most closely aligns with its direction. After completing these two steps, the directional velocity data (DVelocity) and the velocity magnitude data (MVelocity) are mapped onto the corresponding pixels. The resulting DVelocity and MVelocity data sets are converted into three-dimensional(3D) 8-bit images, with intensity values scaled between 0 and 255. More details can be found in our prior publications[6,7].

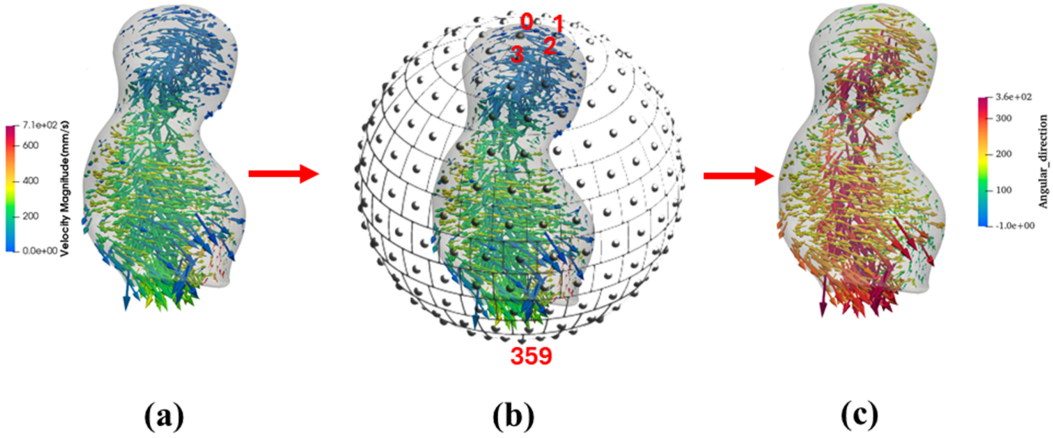

Figure S2. A sequence of three plots showing the process of calculating DVelocity: (a) isolating velocity vectors within IA, (b) utilizing Leopardi's method for defining velocity directions (each partition on the unit sphere corresponds to one unique direction, and (c) computed angular directions for every velocity vector. Recall that all velocity vectors were converted to a rectilinear grid; thus, this process yielded 3D DVelocity images.

Finally, the resultant 3D images representing DVelocity and MVelocity were subjected to detailed quantitative analysis using Pyradiomics[1], a sophisticated Python library tailored for radiomic feature extraction[9]. Pyradiomics provides an extensive array of parameters utilizing various image analysis methods. These include first-order statistics as well as techniques such as the gray level co-occurrence matrix (GLCM)[10], gray level run length matrix (GLRLM)[11], gray level size zone matrix (GLSZM)[12], and gray level dependence matrix (GLDM)[13] which bellow a brief explanation of features utilized in Table 2 of manuscript provided below.

The descriptions of variables computed using GLCM, GLRLM, and GLSZM are similar to those provided in the PyRadiomics documentation[9] and are detailed below for completeness:

`The Gray Level Co-occurrence Matrix (GLCM)` quantifies the spatial relationship between pairs of connected voxels based on their intensity values. It is denoted as $P(i, j \mid \delta, \theta)$, where δ represents the distance between the voxels and θ represents the angle of their relative orientation. The parameter θ takes on one of four discrete values for 2D images and increases to 13 discrete values for 3D images. The Velocity-Informatics varibles computed using GLCM in Table 2 of the manuscript, are explained in Table S2.

For an image (or image-like data) with dimensions $N_x \times N_y$ and N_g different intensity levels, the GLCM is mathematically defined by the following equation[9,10]:

$$\mathrm{GLCM}_{\delta}^{\theta}(i,j) = |\{((r,s),(t,v)) : I(r,s) = i, I(t,v) = j\}| \quad \forall\, i,j \in \{1,2,3,\ldots,N_g\} \tag{3}$$

[1] https://pyradiomics.readthedocs.io/en/latest/

where (t,v) is defined as:

$$(t,v) = \begin{cases} (r+\delta, s) & \text{if } \theta = 0^\circ \\ (r+\delta, s+\delta) & \text{if } \theta = 45^\circ \\ (r, s+\delta) & \text{if } \theta = 90^\circ \\ (r-\delta, s+\delta) & \text{if } \theta = 135^\circ \end{cases}$$

Here, $|\cdot|$ represents the cardinality (number of elements) of a set. $I(r,s)$ and $I(t,v)$ denote the intensity values of the image at positions (r,s) and (t,v) respectively.

Table S2. A summary of velocity-Informatics GLCM variable

Parameter	Descriptions
Difference Average	Quantifies the relationship between the frequency of pairs with similar intensity values and those with differing intensity values. Difference Average $= \sum_{k=0}^{N_g-1} k \cdot p_{x-y}(k)$
Difference Entropy	Quantifies the randomness or variability in the differences between intensity values within a neighborhood. Difference Entropy $= \sum_{k=0}^{N_g-1} p_{x-y}(k) \log_2 \left(p_{x-y}(k)+\varepsilon\right)$
Difference Variance	Quantifies heterogeneity by assigning greater weights to pairs of intensity levels that deviate significantly from the mean. Difference Variance $= \sum_{k=0}^{N_g-1} (k-DA)^2 \cdot p_{x-y}(k)$
Idm	Quantifies the local homogeneity of an image. It assesses how similar intensity values are within neighboring pixel pairs, with higher values indicating greater homogeneity. IDM $= \sum_{k=0}^{N_g-1} \frac{p_{x-y}(k)}{1+k^2}$
Idn	It is a quantitative metric for assessing the local homogeneity of an image. This formula normalizes the intensity value differences between neighboring pixels by dividing by the total number of discrete intensity levels present in the image. This normalization ensures that the measure accounts for variations in intensity ranges, providing a more standardized evaluation of homogeneity. IDN $= \sum_{k=0}^{N_g-1} \frac{p_{x-y}(k)}{1+\frac{k}{N_g}}$
JointEnergy	Quantifies the presence of homogeneous patterns in an image. A higher Energy value indicates that there are more occurrences of neighboring intensity value pairs at higher frequencies throughout the image. JointEnergy=$\sum_{i=1}^{N_g} \sum_{j=1}^{N_g} \left(p(i,j)\right)^2$
JointEntropy	Quantifies the randomness or variability in neighborhood intensity values within an image. It assesses the uncertainty associated with the distribution of paired intensity values in spatially neighboring pixels or voxels. Joint Entropy $= -\sum_{i=1}^{N_g} \sum_{j=1}^{N_g} p(i,j) \log_2(p(i,j)+\varepsilon)$
SumEntropy	Represents the sum of neighborhood intensity value differences within an image. It quantifies the total unpredictability or randomness in the distribution of paired intensity differences across the image. SumEntropy $= \sum_{k=2}^{N_g} p_{x+y}(k) \log_2(p_{x+y}(k)+\varepsilon)$

The Gray Level Run Length Matrix (GLRLM) quantifies the number of connected voxels with the same intensity, characterized by an angle θ between pairs of voxels. Matrix elements $\text{GLRLM}_\theta(i,j)$ denote the number of voxels with intensity i and run length j in the specified direction. The Velocity-Informatics variables computed under the framework of GLRLM in Table 2 of the manuscript, are explained in Table S3.

For an image with dimensions $N_x \times N_y$ and N_g different intensity levels, the GLRLM is mathematically defined by the following equation[9,11]:

$$\text{GLRLM}_\theta(i,j) = \left|\{(m,n) : |\{(k,l) \in \text{Nb}(m,n,j,\theta) : I(k,l) = i\}| > 0\}\right| \quad \forall\, i,j \in \{1,2,3,\ldots,N_g\} \tag{4}$$

where $\mathrm{Nb}(m,n,j,\theta)$ is defined as:

$$\mathrm{Nb}(m,n,j,\theta) = \begin{cases} \{(m+1,n),(m+2,n),\ldots,(m+j,n)\} & \text{if } \theta = 0^\circ \\ \{(m+1,n+1),(m+2,n+2),\ldots,(m+j,n+j)\} & \text{if } \theta = 45^\circ \\ \{(m,n+1),(m,n+2),\ldots,(m,n+j)\} & \text{if } \theta = 90^\circ \\ \{(m-1,n+1),(m-2,n+2),\ldots,(m-j,n+j)\} & \text{if } \theta = 135^\circ \end{cases}$$

Here, $|\cdot|$ denotes the cardinality (number of elements) in a set. $I(k,l)$ represents the intensity of the voxel at position (k,l) in the image.

Table S3. A summary of velocity-Informatics (GLRLM) variable

Parameter	Descriptions
GLN	Measures the similarity of gray-level intensity values within an image. A lower GLN value indicates greater uniformity or similarity in intensity values across the image, implying less variation and a more consistent distribution of gray levels throughout the image. $GLN = \frac{\sum_{i=1}^{Ng}\left(\sum_{j=1}^{Nr} P(i,j\|\theta)\right)^2}{Nr(\theta)}$
LongRunEmphasis	Evaluates the distribution of long-run lengths within a texture. Its higher value indicates a greater prevalence of longer run lengths, suggesting the presence of coarse structural textures characterized by extended homogeneous segments. $\frac{\mathrm{LRE}=\sum_{i=1}^{Ng}\sum_{j=1}^{Nr} P(i,j\|\theta)j^2}{N_r(\theta)}$
LRHGLE	Measures the joint distribution characterized by long run lengths associated with higher gray-level values in an image. $\mathrm{LRHGLRE} = \frac{\sum_{i=1}^{Ng}\sum_{j=1}^{Nr} P(i,j\|\theta)i^2 j^2}{N_r(\theta)}$
RunEntropy	Quantifies the uncertainty or randomness in the distribution of run lengths and gray levels within a texture. Its higher value indicates greater heterogeneity in the texture patterns, reflecting more diverse variations in both the lengths of homogeneous segments and the associated gray levels across the image. $RE = -\sum_{i=1}^{Ng}\sum_{j=1}^{Nr} p(i,j\|\theta)\log_2(p(i,j\|\theta)+\varepsilon)$
RLN	measures the similarity or uniformity of run lengths across the image. Its lower value indicates greater homogeneity among run lengths, suggesting that the lengths of consecutive homogeneous segments in the image are more consistent and less variable. $\mathrm{RLN} = \frac{\sum_{i=1}^{Nr}\left(\sum_{j=1}^{Ng} P(i,j\|\theta)\right)^2}{Nr(\theta)}$
RunPercentage	Measures the coarseness of texture by calculating the ratio of the number of runs to the number of voxels in the ROI. $\mathrm{RP} = \frac{N_r(\theta)}{N_p}$
RanVariance	Measure that quantifies the variance in the lengths of runs within an image. $\mathrm{RV} = \sum_{i=1}^{Ng}\sum_{j=1}^{Nr} p(i,j\|\theta)(j-\mu)^2$, here $\mu = \sum_{i=1}^{Ng}\sum_{j=1}^{Nr} p(i,j\|\theta)j$

Gray Level Size Zone Matrix (GLSZM) was first introduced by Thibault et al.[12] to quantify the distribution of connected regions of voxels with identical intensity levels within an image. In this context, a "zone" is a contiguous cluster of pixels (or voxels in 3D) that share the same intensity value. The element (i,j) in the GLSZM represents the number of zones with an intensity level i and a size j.

A significant advantage of GLSZM over GLCM and GLRLM is that GLSZM does not rely on specific orientations or directions (θ) for its calculation. This orientation independence means that GLSZM generates a unique matrix by considering all possible directions, providing a comprehensive representation of intensity zones in the image. The Velocity-Informatics variables computed using GLSZM in Table 2 of the manuscript are explained in Table S4.

Table S4. A summary of velocity-Informatics GLSZM variable

Parameter	Descriptions
LargeAreaEmphasis	evaluates the distribution of large-size zones within an image where a greater value shows more coarse textures. $\mathrm{LAE} = \frac{1}{N_z}\sum_{i=1}^{N_g}\sum_{j=1}^{N_s} P(i,j)\,j^2$
LAHGLE	Quantify the proportion in the image of the joint distribution of larger size zones with higher gray-level values. $\mathrm{LAHGLE} = \frac{1}{N_z}\sum_{i=1}^{N_g}\sum_{j=1}^{N_s} P(i,j)\,i^2\,j^2$
SizeZoneNonUniformity	Quantifies the variability of size zone volumes within an image. Its lower value indicates a more homogeneous distribution of zone sizes, reflecting uniformity in the volume distribution across the texture. $\mathrm{SZN} = \frac{1}{N_z}\sum_{j=1}^{N_s}\left(\sum_{i=1}^{N_g} P(i,j)\right)^2$
SmallAreaEmphasis	Evaluates the distribution of small-size zones within a texture. Its higher value suggests a higher prevalence of smaller size zones and finer textures, highlighting the presence of intricate details and finer variations in the image texture. $\mathrm{SAE} = \frac{1}{N_z}\sum_{i=1}^{N_g}\sum_{j=1}^{N_s} \frac{P(i,j)}{j^2}$
ZoneEntropy	Quantifies the uncertainty or randomness in the distribution of zone sizes and gray levels. $\mathrm{ZE} = -\sum_{i=1}^{N_g}\sum_{j=1}^{N_s} p(i,j)\log_2\left(p(i,j)+\varepsilon\right)$
ZonePercentage	Measures the coarseness of texture by calculating the ratio of the number of zones to the number of voxels in the Region of Interest (ROI). $\mathrm{ZP} = \frac{N_z}{N_p}$
ZoneVariance	Measures the variance in gray level intensities within the zones. $\mathrm{ZV} = \sum_{i=1}^{N_g}\sum_{j=1}^{N_s} p(i,j)(j-\mu)^2$,here $\mu = \sum_{i=1}^{N_g}\sum_{j=1}^{N_s}$

S4 Visual Assessments of Gross Hemodynamics with IAs Over A Cardiac Cycle

Time-resolved results from the additional three cases (see Figs. 7 and 8) in the manuscript are provided below for the sake of completeness.

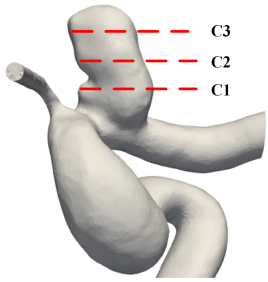

(a)

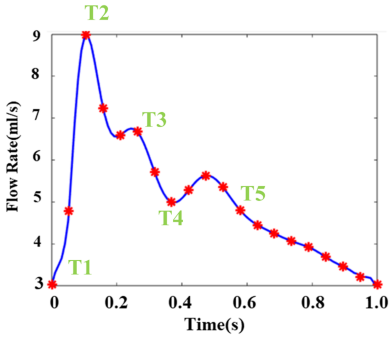

(b)

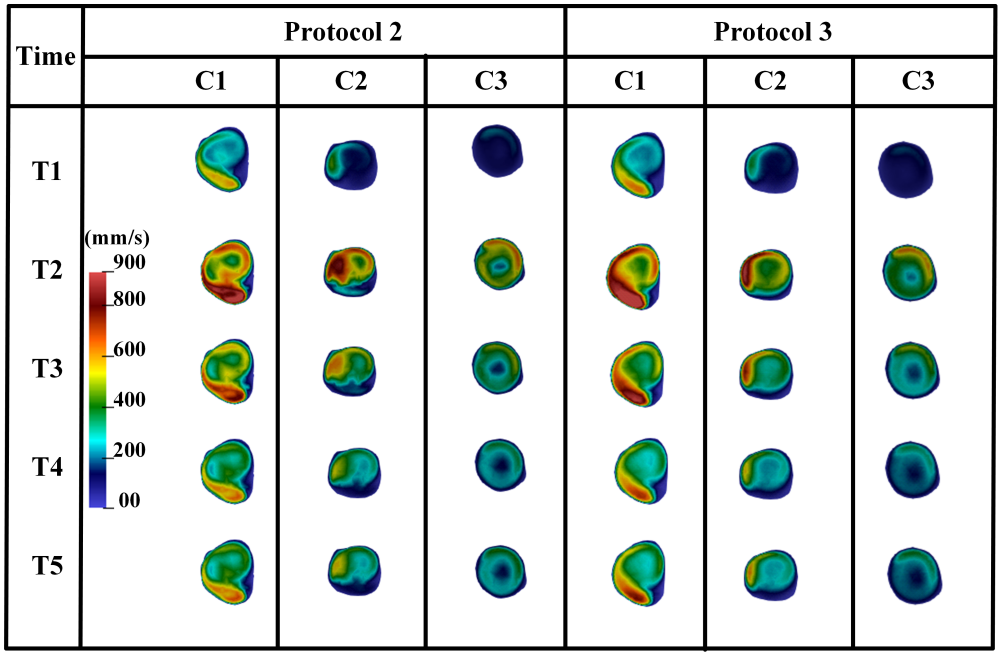

(c)

Figure S3. Comparison of velocity magnitude: Manual vs. automated workflow across different cardiac phases: (a) IA Geometry and cross-sectional cutting plans,(b) a Flow rate waveform,(c) Velocity magnitude contour at specific cross-sectional cutting planes (see (a)) and cardiac phases (see (b))

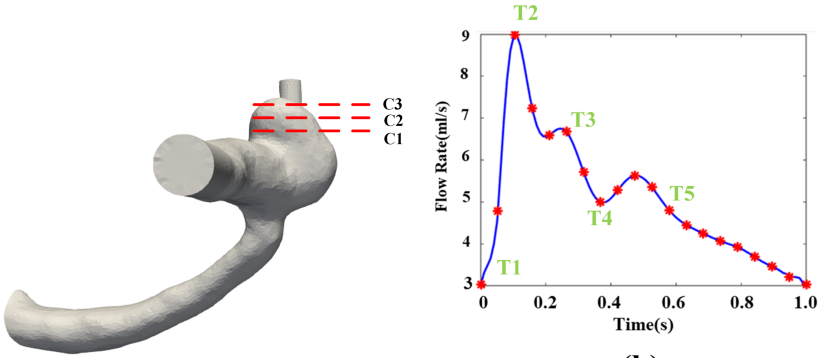

(b)

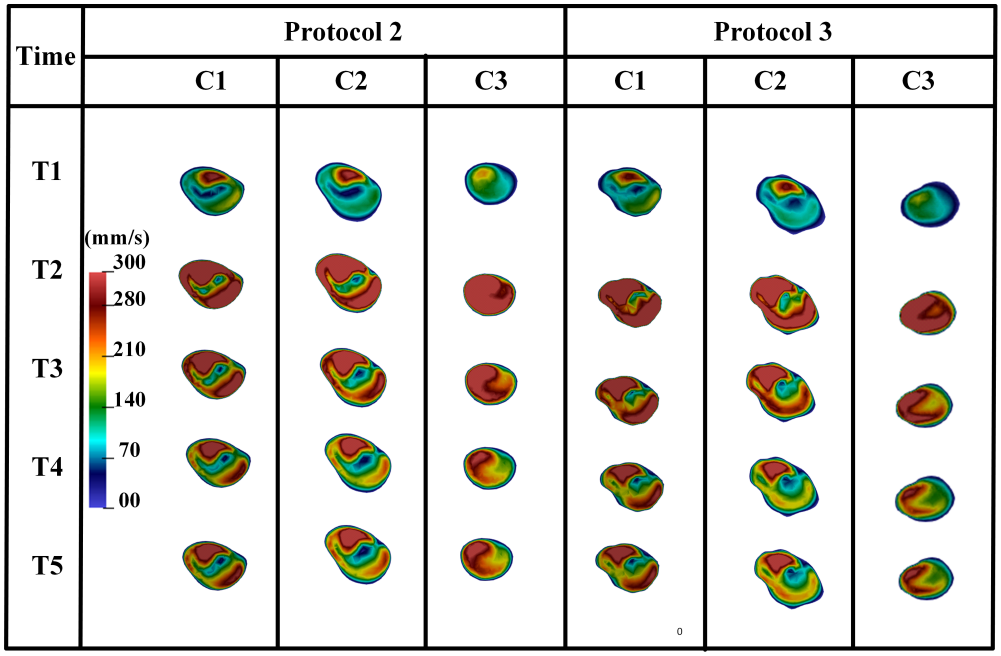

(c)

Figure S4. Comparison of velocity magnitude: Manual vs. automated workflow across different cardiac phases: (a) IA Geometry and cross-sectional cutting plans,(b) a Flow rate waveform,(c) Velocity magnitude contour at specific cross-sectional cutting planes (see (a)) and cardiac phases (see (b))

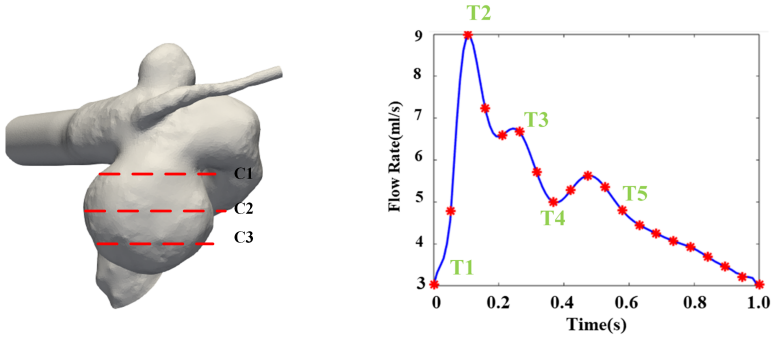

(a) (b)

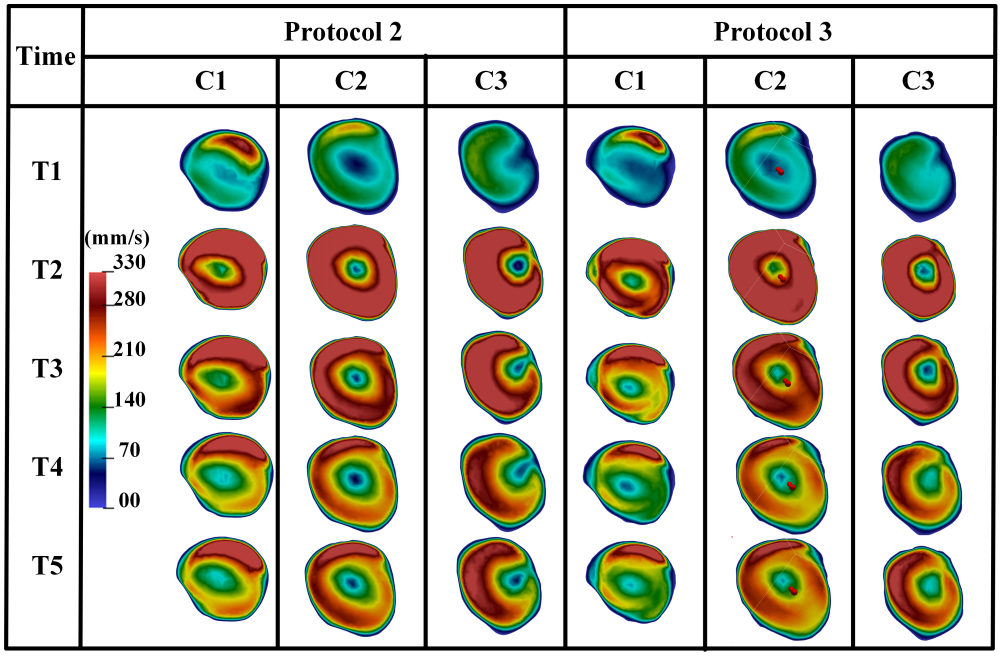

(c)

Figure S5. Comparison of velocity magnitude: Manual vs. automated workflow across different cardiac phases: (a) IA Geometry and cross-sectional cutting plans,(b) a Flow rate waveform,(c) Velocity magnitude contour at specific cross-sectional cutting planes (see (a)) and cardiac phases (see (b))

References

1. Jiang, J. & Strother, C. M. Interactive decomposition and mapping of saccular cerebral aneurysms using harmonic functions: its first application with "patient-specific" computational fluid dynamics (cfd) simulations. *IEEE transactions on medical imaging* **32**, 153–164 (2012).
2. Piccinelli, M., Veneziani, A., Steinman, D. A., Remuzzi, A. & Antiga, L. A framework for geometric analysis of vascular structures: Application to cerebral aneurysms. *IEEE Transactions on Med. Imaging* **28**, 1141–1155, DOI: 10.1109/TMI.2009.2021652 (2009).
3. Katritsis, D. *et al.* Wall shear stress: theoretical considerations and methods of measurement. *Prog. cardiovascular diseases* **49**, 307–329 (2007).
4. Qin, H. *et al.* Morphological and hemodynamic parameters for middle cerebral artery bifurcation aneurysm rupture risk assessment. *J. Korean Neurosurg. Soc.* **60**, 504 (2017).
5. He, X. & Ku, D. N. Pulsatile Flow in the Human Left Coronary Artery Bifurcation: Average Conditions. *J. Biomech. Eng.* **118**, 74–82, DOI: 10.1115/1.2795948 (1996). https://asmedigitalcollection.asme.org/biomechanical/article-pdf/118/1/74/5504426/74_1.pdf.
6. Jiang, J. *et al.* Augmenting prediction of intracranial aneurysms' risk status using velocity-informatics: Initial experience. *J. cardiovascular translational research* 1–13 (2023).
7. Rezaeitaleshmahalleh, M. *et al.* Characterization of small abdominal aortic aneurysms' growth status using spatial pattern analysis of aneurismal hemodynamics. *Sci. reports* **13**, 13832 (2023).
8. Leopardi, P. A partition of the unit sphere into regions of equal area and small diameter. *Electron. Transactions on Numer. Analysis* **25**, 309–327 (2006).
9. Van Griethuysen, J. J. *et al.* Computational radiomics system to decode the radiographic phenotype. *Cancer research* **77**, e104–e107 (2017).
10. Haralick, R. M., Shanmugam, K. & Dinstein, I. H. Textural features for image classification. *IEEE Transactions on systems, man, cybernetics* 610–621 (1973).
11. Galloway, M. M. Texture analysis using gray level run lengths. *Comput. graphics image processing* **4**, 172–179 (1975).
12. Thibault, G., Angulo, J. & Meyer, F. Advanced statistical matrices for texture characterization: application to cell classification. *IEEE Transactions on Biomed. Eng.* **61**, 630–637 (2013).
13. Sun, C. & Wee, W. G. Neighboring gray level dependence matrix for texture classification. *Comput. Vision, Graph. Image Process.* **23**, 341–352 (1983).